Pattern Formation in *Passiflora Incarnata*: an Activator-Inhibitor Model

Agastya P. Bhati*, S. Goyal†, Ram Yadav† and N. Sathyamurthy†
*Centre for Computational Science, Department of Chemistry,
University College London, London, United Kingdom
†Indian Institute of Science Education and Research Mohali,
Sector 81, SAS Nagar, Manauli 140306 India
Email: nsath@iisermohali.ac.in
Phone: +91-9779144905

Abstract

Based on a careful examination of the onset of violet colored dots along the filaments in the developing floral bud stage and the formation of alternating bands of violet and white color in the matured flowers of *Passiflora incarnata* (Passion flower), it is concluded that the pattern arises from a competition between the production of violet colored anthocyanin and the colorless flavonols along the filaments. The activator-inhibitor model of Gierer and Meinhardt along with the reaction diffusion theory of Turing is used to explain the formation of concentric rings in the flower.

1 Introduction

Biological world is rich with attractive patterns and symmetry (Ball 2016). These may be in the form of differently shaped structures of organisms or coloured designs on their skins/surfaces. The genesis of such patterns in Nature is of fundamental interest, not only to the specific cases where such patterns are observed, but also in understanding of several phenomena in both natural and man made systems. At what stage of an organism's development does a pattern start emerging and when does it completely set in is a question that is not fully answered. Turing, in his seminal paper in 1952 (Turing 1952), proposed the Reaction-Diffusion (RD) theory to explain the chemical basis of morphogenesis. He devised a mathematical model for the mechanism of morphogenesis from a mixture of chemicals (morphogens) which react together and diffuse through the tissues. Turing demonstrated theoretically that a homogeneous mixture of such chemicals could lead to spatial patterns of their concentrations triggered by random fluctuations. Rashevsky (Rashevsky 1961) invoked diffusion as a fundamental process at the cellular level. He also invoked the idea of excitation and inhibition to account for the shapes of biological entities.

A more general and refined form of the reaction diffusion equation, derived from its original form proposed by Turing is (Murray 2003)

$$\frac{\partial \boldsymbol{u}}{\partial t} = \boldsymbol{D}\nabla^2\boldsymbol{u} + \boldsymbol{f}(\boldsymbol{u}, \boldsymbol{p}), \tag{1}$$

where $\boldsymbol{u}$ is a vector of chemical concentrations, $\boldsymbol{D}$ is the matrix of diffusion coefficients and $\boldsymbol{f}$ is a chemical coupling matrix with kinetic parameters $\boldsymbol{p}$.

Considering only two variables A and I to represent activator and inhibitor, respectively, in equation (1), we obtain

$$\frac{\partial A}{\partial t} = D_A\nabla^2 A + f(A, I) \tag{2a}$$

$$\frac{\partial I}{\partial t} = D_I\nabla^2 I + g(A, I), \tag{2b}$$

Using linear functions as the coupling terms in his equations, Turing solved the equations analytically and found exponentially growing concentration values, which are unrealistic. Subsequently, several workers have proposed different models for the kinetic coupling in equation (2). Perhaps, two most popular ones are by Thomas (Thomas and Kernezev 1975) and Gierer and Meinhardt (Gierer and Meinhardt 1972) and are the following:

Thomas kinetics (adopted by Murray (Murray 2003)):

$$f(A, I) = k_1 - k_2 A - h(A, I) \tag{3a}$$

$$g(A, I) = k_3 - k_4 I - h(A, I), \tag{3b}$$

$$h(A, I) = \frac{k_5 AI}{k_6 + k_7 A + k_8 A^2}. \tag{3c}$$

where k_1,...., k_8 are the rate coefficients.

Gierer-Meinhardt kinetics (activator-inhibitor model):

$$f(A, I) = \frac{\rho A^2}{I} - \mu A + \rho_0 \tag{4a}$$

$$g(A, I) = \rho' A^2 - \nu I. \tag{4b}$$

where ρ, ρ', ρ_0, μ and ν are the different rate coefficients involved. It is important to add here that the A^2 term represents the autocatalytic role of A and the inhibitor I tries to control it. Both versions of kinetic equations have been used successfully to understand the mechanism, at the molecular level, of various biological phenomena and patterns such as, cartilage formation in vertebrate limbs, coloured patterns of butterfly wings, alligator teeth, head regeneration in hydra, spots of cheetah, stripes of zebra, patterns on sea shells and many more (Murray 2003; Meinhardt 1982; 2009).

Kondo and Asai (Kondo and Asai 1995) had shown that the stripe patterns on the skin of the marine angelfish, *Pomacanthus*, could be explained in terms of the RD model, invoking an activator and an inhibitor (Meinhardt 1995). The key element in their study was the observation that the patterns were not fixed and that the number of morphogen peaks doubled in a growing one dimensional pattern. Painter *et al.* (Painter et al. 1999) proposed a generalized Turing model taking into account the growth and movement in cells to explain the nuances of the observed patterns in *Pomacanthus semicirculatus*. Specifically, they were able to mimic the pattern formation not only along the length and breadth of the fish but also close to its tail and fins as the fish grows. Kondo and Miura (Kondo and Miura 2010) reviewed the work done over the years using the RD model to explain the formation of various patterns. While a gradient in a single morphogen could lead to a one-dimensional (1D) vertical or horizontal stripes, two noninteracting morphogens could result in two-dimensional (2D) waves. However, an interaction between two morphogens could be the source of more complex patterns. A modified RD model with different combinations of parameters could account for a variety of patterns that are observed in nature. Singh and Nüsslein-Volhard (Singh and Nüsslein-Volhard 2015) examined the different stripes formed on the skin of the zebrafish and concluded that they arose from a combination of (seven) different color pigments.

Winfree (Winfree 1972) had demonstrated the formation of spiral waves (in space) in the Belousov-Zhabotinskii reaction that exhibits temporal oscillations (Field and Noyes 1977). A prerequisite for such oscillations is an autocatalytic or a feedback mechanism. In addition to showing that diffusion and feedback can lead to self-organization and varied pattern formation, van Roekel *et al.* (van Roekel et al. 2015) have reviewed a variety of works that demonstrate how programmable chemical reaction networks pave the way for the development of cell-free sensors.

We have reported recently (Goyal et al. 2019) on the discovery of synchronous pulsed flowering in Passion flower, *Passiflora incarnata (PI)*. While the synchronicity in flowering between different

plants remains to be explained, temporal oscillations in flowering in individual plants was explained in terms of a modified Lotka model (Lotka 1910). The model comprised a florigen (Chailakhyan 1936), that is responsible for flowering and an antigen (Lang and Melchers 1943) that works against flowering. Although the florigen and the anti-florigen responsible for the temporal oscillations in PI flowering remain to be identified in biochemical terms, the former plays an autocatalytic role and the latter an inhibitory role. In this study, we have applied an RD model to qualitatively understand the spatial distribution of florigen and anti-florigen in PI. It should be noted that we have not attempted to quantitatively reproduce the exact pattern here.

The breathtaking beauty of Passion flower lies partly in the characteristic alternation of violet and white bands in each one of them as illustrated in Figure 1a. The observation of such concentric bands in chemical systems is reminiscent of Liesegang rings (McGuigan and Brough 1923; Stern 1954; Krug and Brandtstädter 1999) formed during the precipitation of silver dichromate from silver nitrate and potassium dichromate solutions in a gel. Bhatnagar and Sehgal had invoked the same mechanism for explaining the formation of rings in beet roots (Bhatnagar and Sehgal 1926).

(a) The photograph (top view) of a representative sample of *Passiflora Incarnata* (passion flower) taken from the garden of the Director's residence in IISER Mohali by one of the authors (NS).

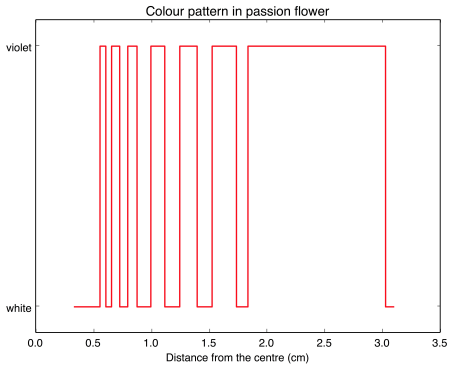

(b) Alternation of white and violet colour bands in the representative sample.

Figure 1: Pattern formation in a Passion flower

Since it is not possible to monitor in real time the formation of the violet bands in a Passion flower, we cut open the developing floral buds to determine at which stage colored stripes develop in the filaments during flower development. The smallest (and presumably the youngest) flower bud revealed tender and colorless filaments as illustrated in Fig. 2a. In a slightly older bud (Fig. 2b), the filaments remain colorless. As the floral buds start growing in size, the male and female reproductive organs mature and spots of violet color begin to appear on the filaments, which become distinctly visible prior to blooming as illustrated in Fig. 2c, 2d and 2e. In a matured bud, the color bands begin to appear as shown in Fig. 3a. A magnified view of individual filaments reveals bead like structures with violet and white colours as illustrated in Fig. 3b. As each filament grows in length and size, the intensity of violet color increases and the formation of bands is completed on maturity as illustrated in several panels in Figure 2 and Figure 3.

UV-vis spectral and mass spectral studies of the methanol extract of the filaments of Passion flower revealed the violet color to be due to anthocyanins (Ramasastry et al. 2021).

From a color print of a high resolution picture of a representative Passion flower in IISER Mohali campus (see Figure 1a), the width of each successive colour band was measured for 21 filaments. The

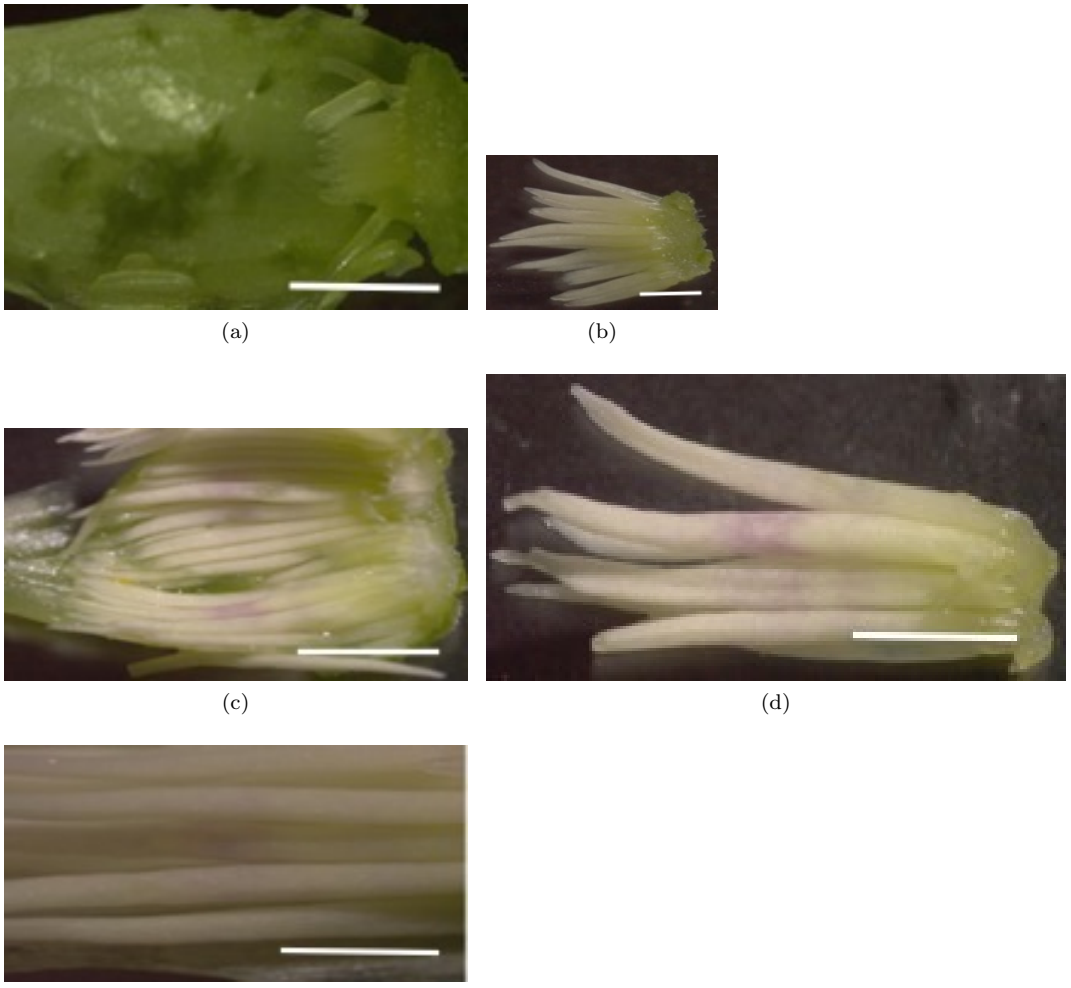

Figure 2: Different stages in the development of the filaments and the onset of violet color. Panels (a) and (b) show tender colorless filaments, while (c), (d), and (e) show different levels of growth in the filaments and the violet spots developing along the length of the filament. The scale bar inserted in each panel corresponds to 250 microns (0.25 mm).

average width of each colour band was plotted against the distance from the centre to obtain the pattern shown in Figure 1b. We have obtained this representative pattern from filaments of only a single flower to get a qualitative picture. Incidentally, the average length of a filament in a matured flower is 3.1 cm.

An important feature of this pattern is that the color distribution is radial and the rings are concentric. The width of different color bands is nearly uniform across filaments and non-uniform along the length of each filament (See Fig 4 and Table 1). The width of the violet band keeps on increasing on moving towards the tip of the filament. The width of the white bands, on the other hand, increases initially, then decreases and then increases, but eventually becomes nearly zero on moving towards the tip of the filaments. As we move to larger distances from the centre, the violet colour dominates. However, the tail end of each filament becomes white. It is important to reiterate that the base of the filament is white.

Table 1: Measured pattern of alternating colour bands in a sample Passion flower; W: White, V: Violet

Colour of the circle	Distance from the centre	Width of the band
Red	0.34	0.34
W1	0.56	0.22
V1	0.61	0.05
W2	0.66	0.05
V2	0.73	0.07
W3	0.80	0.07
V3	0.88	0.08
W4	1.00	0.12
V4	1.12	0.12
W5	1.25	0.13
V5	1.40	0.15
W6	1.53	0.13
V6	1.74	0.21
W7	1.84	0.10
V7	3.03	1.17
W8	3.10	0.07

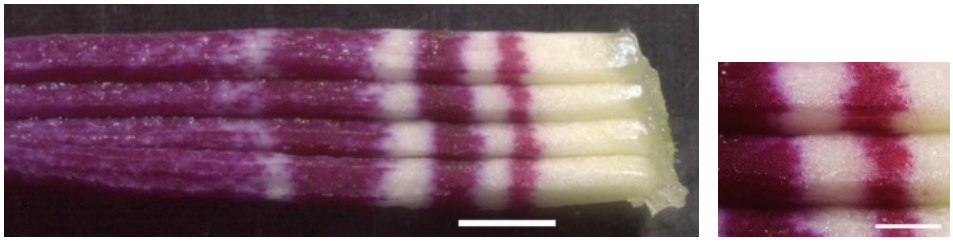

(a) (b)

Figure 3: (a) A close up view of the alternating white (at the base of the filament) and violet color bands along the filaments in a matured flower. (b) A magnified image of the individual filaments showing the bead like structure and colors. Scale bar in (a) corresponds to 250 microns, while that in (b) corresponds to 18 microns.

It has been shown recently by Yuan et al (Yuan et al. 2016) that the stripes in monkey flower could arise from a competition between the biosynthesis of pink colored anthocyanin and the colorless flavonoids. At the molecular level, this is achieved by the activation of flavonol synthase gene, which takes away the anthocyanin intermediate.

A similar mechanism could be responsible for the formation of stripes in PI. Although the biochemical pathways for the production of flavonols and anthocyanins in PI are not identified yet, it is reasonable to conclude that when the flowering is initiated by the florigen, flavonols and anthocyanins are synthesized, albeit in small quantities, before the onset of violet color along the filaments in floral buds. In the language of the activator-inhibitor model, we identify the colorless flavonol to be the inhibitor spread across the length of the filaments. We identify the violet-colored anthocyanin as the activator (or the outcome of the activator) that begins to show up in increased measures as the bud grows. But its movement along the length of the filament would be resisted by the flavonol resulting in an alternation of white-violet-white. . . -violet-white bands.

Hearn (Hearn 2019) has used the Turing-like mechanism in a reaction-diffusion model to recreate three-dimensional vascular patterning of plant stems. In his model, the activator diffuses radially, away from the centre and its expansion is restricted by the inhibitor.

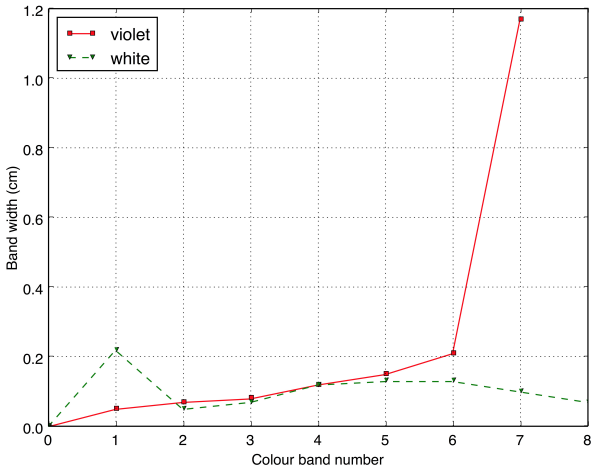

Figure 4: Variation in widths of violet and white colour bands in PI.

Although we could have adopted a two-dimensional model in polar coordinates, with the activator and the inhibitor originating at the centre and spreading radially, to investigate the band formation in PI, we have used a one-dimensional model (along the radial direction), to start with, for understanding the formation of color bands in PI.

2 Model study

In this study, we have adopted the Gierer-Meinhardt kinetics (eq. 4). Since the concentric rings are nearly circular, azimuthal symmetry was assumed and the kinetic equations were solved in one dimension (x):

$$\frac{\partial A}{\partial t} = \frac{\rho A^2}{I} - \mu A + D_A \frac{\partial^2 A}{\partial x^2} + \rho_0 \tag{5a}$$

$$\frac{\partial I}{\partial t} = \rho' A^2 - \nu I + D_I \frac{\partial^2 I}{\partial x^2}, \tag{5b}$$

where A is the activator concentration, I is the inhibitor concentration, ρ, μ and ν are first order rate coefficients, ρ' is a second order rate coefficient, D_A and D_I are diffusion coefficients of the activator and the inhibitor, respectively. We would like to mention here that we had carried out 2D calculations also. But the results were indistinguishable from those obtained using the 1D model because of the azimuthal symmetry of the system.

As a first step in our study, we decided to use realistic values of different parameters in appropriate units. In a study conducted jointly by the U.S. Fish and Wildlife Service and the U.S. Atomic Energy Commission (Williams and Murdoch 1966), it was found that the average concentration of Chlorophyll a in Phytoplankton (a type of microalgae) over an year's span was of the order of a few μg L^{-1}, which is equivalent to a few nmol L^{-1}. Since the violet colour in PI arises from anthocyanin and the white color from flavonols, the values of A and I are taken in nmol L^{-1} (nM) units. The diffusion coefficient of Rhodamine 6G (a dye) in 50/50 methanol/water solution is known to be 2.7 x

10^{-6} cm^2 s^{-1} (Culbertson et al. 2002). The diffusion coefficient of protein, DNA or other biological molecules in cellular media is expected to be a few orders of magnitude smaller than this. The diffusion coefficient of a DNA molecule in *E. coli* is found to be of the order of 10^{-9} cm^2 s^{-1} (Winter et al. 1981). We have used the values of D_A and D_I of the order of 10^{-2} to 10^{-1} μm^2 s^{-1}. It is worth mentioning here that D_I is taken to be larger than D_A as the inhibitor needs to diffuse faster than the activator to yield concentration patterns. Experimentally, the value of the first order rate coefficient for protein-DNA reaction in *E. coli* is known to be of the order of 10^{-2} s^{-1} and that of the second order diffusion-controlled rate coefficient is of the order of 10^7 M^{-1} s^{-1} (Winter et al. 1981). Therefore, we have taken these values to be of the order of 10^{-2} s^{-1} and 10^{-2} nM^{-1} s^{-1} respectively.

It is worth emphasizing that the choice of parameters is by no means unique. The relative values of A and I, D_A and D_I and the rate coefficients are likely to influence the emerging pattern.

For an initial investigation, we have considered a one dimensional model for a single filament. We have taken a linear array of 3000 cells (along x direction with x ranging from 1 to 3000 microns), with the cell number 1 considered to be at the base of the filament. We have considered a constantly growing domain, starting with 300 microns (800 microns in case of initial conditions 5 and 6 or IC5 and IC6), increasing it by 300 microns after every 7000 s, up to a maximum of 3000 microns (not shown).

We have studied the evolution of the activator and inhibitor concentrations for different sets of initial conditions (see below). Values of the parameters are taken as follows: $\mu = 0.01$ s^{-1}, $\nu = 0.02$ s^{-1}, $\rho = 0.01$ s^{-1}, $\rho' = 0.01$ s^{-1} nM^{-1}, $\rho_0 = 0.00001$ nM s^{-1}, $D_A = 0.02$ μm^2 s^{-1}, $D_I = 0.4$ μm^2 s^{-1} (20 times D_A). The initial concentration of A and I are taken to be: $A_0 = 2.001$ nM and $I_0 = 2.002$ nM.

We, hereafter, denote the activator and inhibitor concentrations in cell number i as A[i] and I[i] respectively. Initial Condition 1 (IC1) has a high concentration at one end of the array of cells with a uniform steady state over the rest of the cells as follows: $A[1] = 2001$ nM ($1000A_0$), A[i] $= A_0$ (i = 2 to 3000), I[i] $= I_0$ (i = 1 to 3000). Thus $A[1]$ /$I[1] = 2001$.

Initial condition 2 (IC2) has a slightly higher concentration at one end, gradually approaching the uniform steady state with an increase in the cell number as follows: $A[1] = I[1] = 15$ nM, thereafter gradually decreasing in steps of 1 nM with increasing cell number up to $A[13] = I[13] = 3$ nM, and then uniform steady state A[i] $= A_0$, I[i] $= I_0$ (i = 14 to 3000). Ratio $A[1]/I[1] = 1$.

When the initial concentrations of A and I in IC1 and IC2 were set as nearly equal, the simulated width of the violet/white bands was uniform (see below) and did not reproduce the observed non-uniform widths of violet and white bands. To understand the underlying causes of nonuniform band widths in the flower, the relative values of A and I and that of D_A and D_I were varied as described in the next section.

Numerical methods were employed to solve the equation (5) as they are analytically not solvable due to the presence of the non-linear coupling terms. The 3-point finite difference formula was used to evaluate the second order spatial derivative and the Crank-Nicholson scheme was employed for time evolution (Bhati 2014).

3 Results and Discussion

The system under consideration was evolved spatially and temporally using numerical methods mentioned above for chosen initial conditions for 150000 time steps ($\triangle x = 1$ micron and $\triangle t = 1$ s).

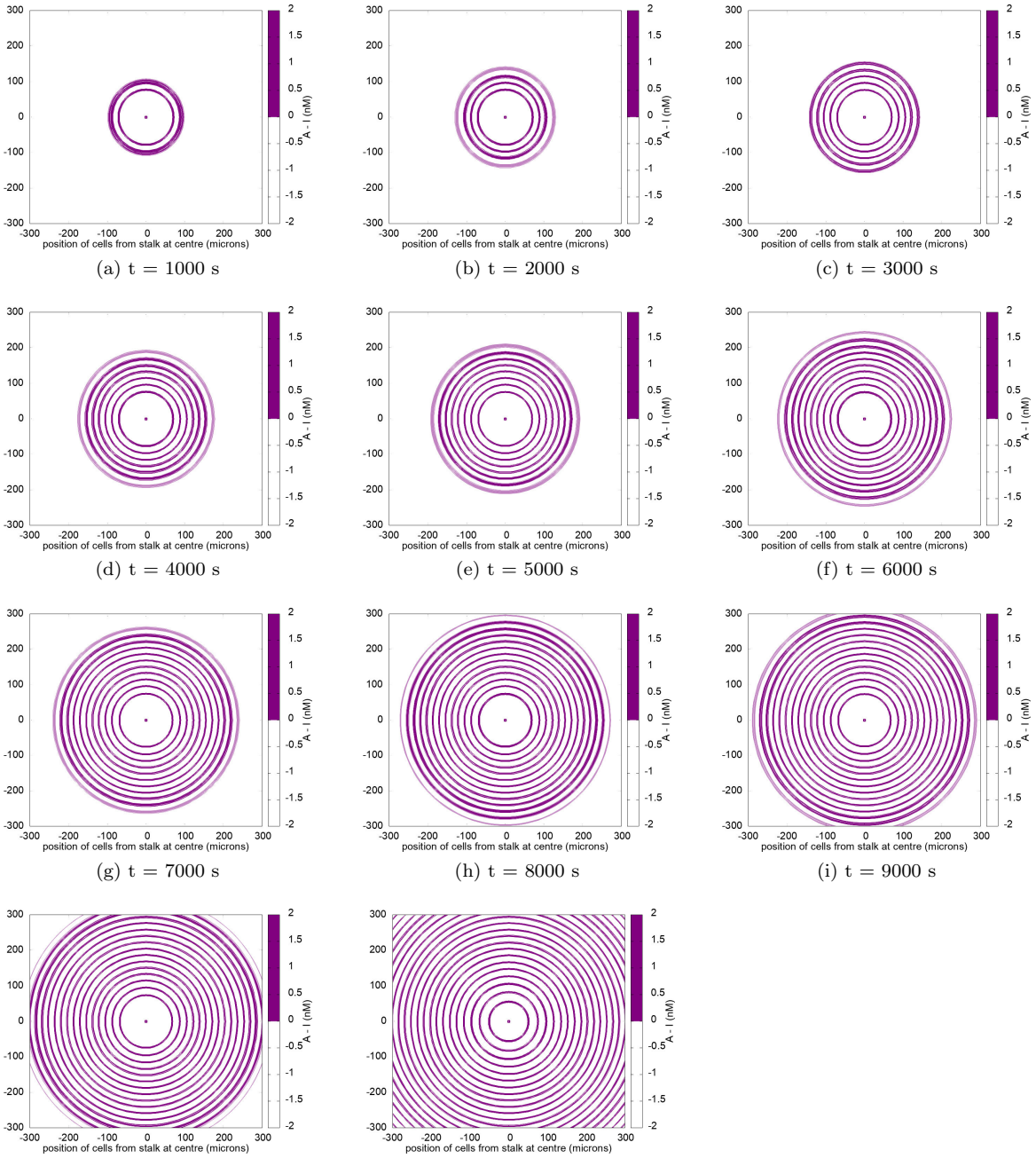

(a) t = 1000 s (b) t = 2000 s (c) t = 3000 s

(d) t = 4000 s (e) t = 5000 s (f) t = 6000 s

(g) t = 7000 s (h) t = 8000 s (i) t = 9000 s

(j) t = 10000 s (k) t = 80000 s

Figure 5: Spatio-temporal evolution of the system in (x, y) coordinates for the initial condition IC1.

In the case of IC1, the concentration of the activator in cell number 1 is 1000 times larger than that in other cells. Due to such a high concentration of the activator, more activator is produced due to self activation. The concentration of the inhibitor also increases rapidly due to activation. Due to the higher diffusivity of the inhibitor, it inhibits the production of the activator, and itself in the neighboring cells. With an increase in time, an alternation of concentration of A and I sets in and spreads to other cells, eventually giving rise to an alternation of concentration of A and I as illustrated in Figure 5. This feature is clearly visible in Figure 6 as a long valley between the first

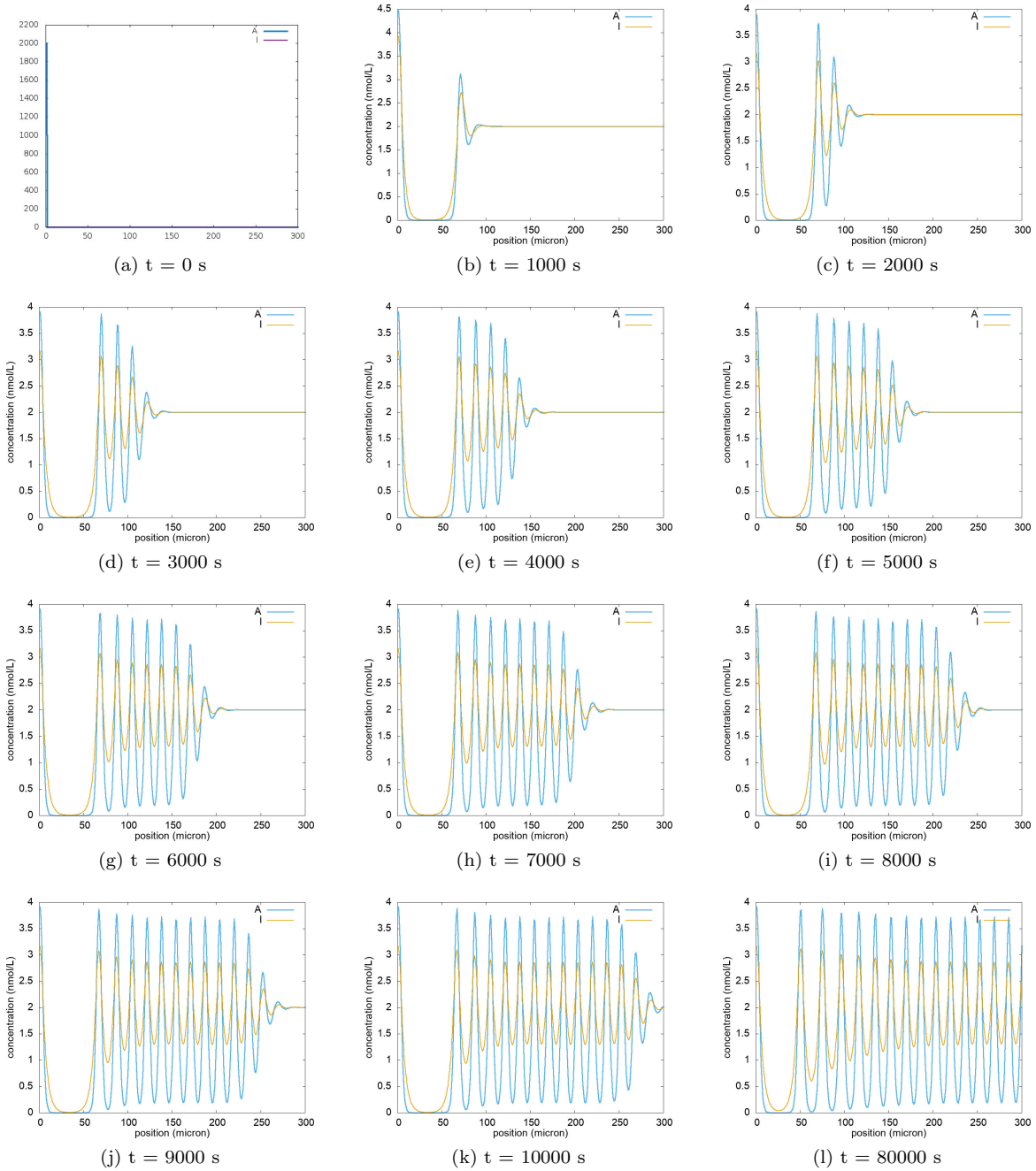

(a) t = 0 s (b) t = 1000 s (c) t = 2000 s

(d) t = 3000 s (e) t = 4000 s (f) t = 5000 s

(g) t = 6000 s (h) t = 7000 s (i) t = 8000 s

(j) t = 9000 s (k) t = 10000 s (l) t = 80000 s

Figure 6: Variation of the concentration of A and I with time along the x-axis for the initial condition IC1, $D_I/D_A = 20$, with concentration (nM) plotted along the y-axis

two peaks in the concentration profile.

In the case of IC2, the feature of the valley between the first two peaks is not much pronounced as the initial concentration in the cells at one end is not very high when compared to nearby cells. In general, a higher initial concentration at one end quickly spreads over the whole length, as illustrated in Figure 7. This feature is expected due to the coupling terms in equation (5). Another consequence

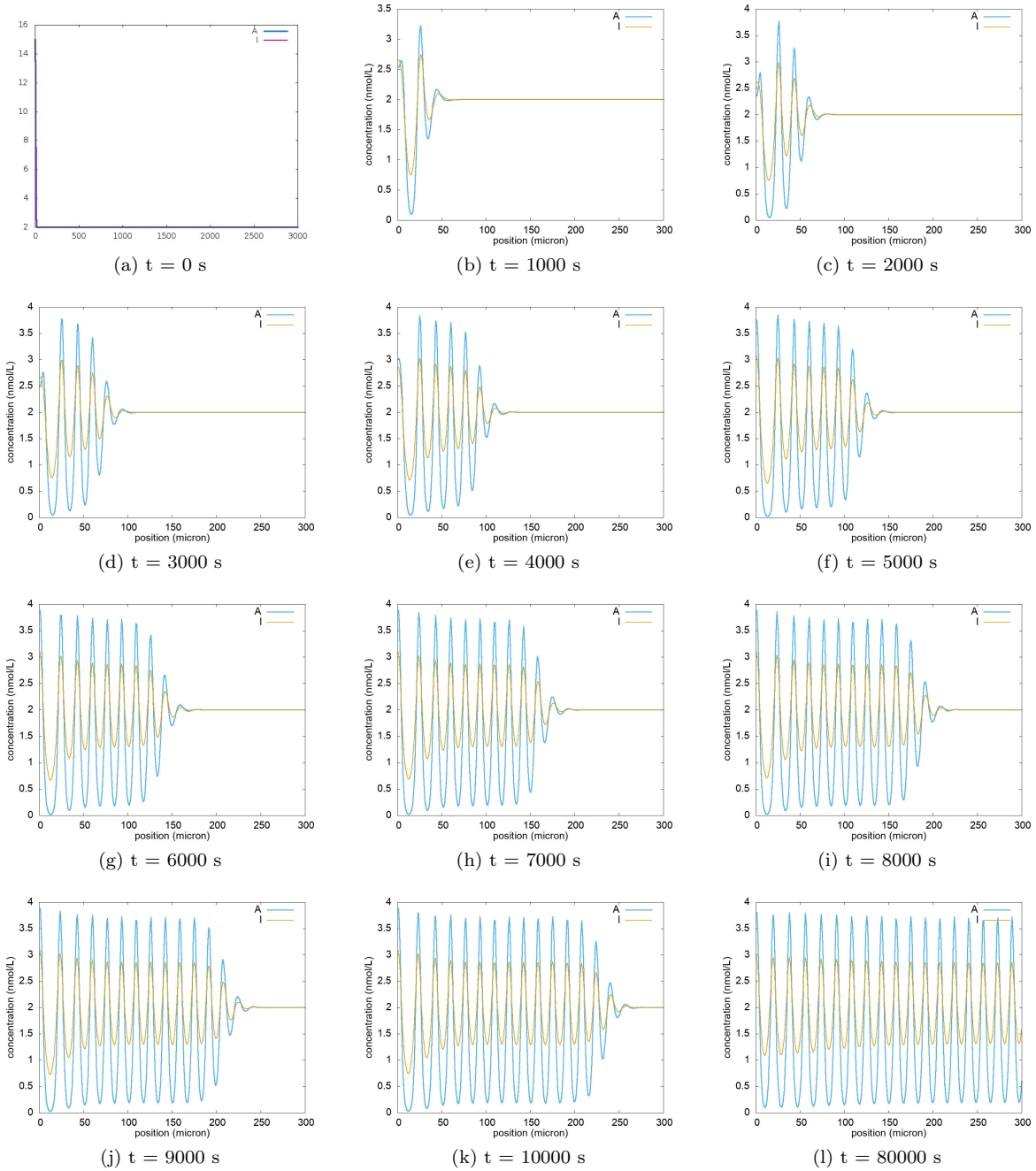

(a) t = 0 s (b) t = 1000 s (c) t = 2000 s

(d) t = 3000 s (e) t = 4000 s (f) t = 5000 s

(g) t = 6000 s (h) t = 7000 s (i) t = 8000 s

(j) t = 9000 s (k) t = 10000 s (l) t = 80000 s

Figure 7: Same as Figure 6 for the initial condition IC2.

of such a coupling is the concentration pattern oscillating in space, which is a characteristic of the activator-inhibitor model.

In general, we observe oscillating concentration values for both the activator and the inhibitor. Notably, the amplitude of the oscillation of the activator is larger than that of the inhibitor. This is the reason for the activator concentration being larger at crests and smaller at troughs than the inhibitor concentration.

Since the observed pattern in PI (see Figure 1(a) and Figure 1(b)) consists of alternating violet and white colours with non-uniform band widths, simulations of the patterns were carried out for various initial concentrations of A and I and diffusion rates. To see if concentric rings are formed, the same colour code is used to plot our results in the form of circles with the computed linear pattern considered as radial as illustrated in Figure 5 for IC1.

It is clear from Figures 6 and 7 that different initial conditions yield slightly different patterns evolving in space and time. Although the concentric ring pattern evolving from our calculations is not exactly the same as observed in nature, it appears that the activator-inhibitor model of RD theory could account for the pattern in PI, if appropriate parameter values and initial conditions are chosen.

Therefore, we have considered variations in the values of the relative concentrations of A and I and the relative values of D_A and D_I as follows:

IC3: $A[1]$=200 nM and $I[1]$=20 nM (ratio 1:0.1), and then both values of A and I decrease in steps of 1 nM at each adjacent cell, to finally reach the values of $A_0 = 2.001$ nM and $I_0 = 2.002$ nM.

IC4: $A[1]$=20 nM and $I[1]$=200 nM (ratio 1:10), and then both values of A and I decrease in steps of 1 nM at each adjacent cell, to finally reach the values of $A_0 = 2.001$ nM and $I_0 = 2.002$ nM.

IC5: $A[1]$=400 nM and $I[1]$=20 nM (ratio 1:0.05), and then both values of A and I decrease in steps of 1 nM at each adjacent cell, to finally reach the values of $A_0 = 2.001$ nM and $I_0 = 2.002$ nM.

IC6: $A[1]$=20 nM and $I[1]$=400 nM (ratio 1:20), and then both values of A and I decrease in steps of 1 nM at each adjacent cell, to finally reach the values of $A_0 = 2.001$ nM and $I_0 = 2.002$ nM.

The results of the variation in the concentration of A and I with increase in time are illustrated in Figure 8 for t = 1000, 2000 and 3000 s. Clearly a variation in the ratio of the initial concentrations of the activator and the inhibitor brings about a variation in the band width for the different colours.

The influence of the ratio of the diffusion coefficients for the activator and the inhibitor on the time evloution of the system and hence the bandwidth for the distribution of the activator (violet) and the inhibitor (white) is illustrated in Figure 9 for D_I/D_A = 5, 10, 20 and 40 for the initial concentration IC6. A larger diffusion coefficient for the inhibitor is critical for the observation of bimodal and trimodal distribution of colors in PI.

Our investigations reveal that the band formation in PI is dependent on the relative values of μ and ν also. While at this stage, it is possible to simulate the non-uniformity of colour bands in PI through variations in the initial conditions of diffusion coefficients and ratios of concentrations of the activator and the inhibitor, to reproduce precisely the observed morphology of PI, further investigations will be required.

4 Summary and Conclusion

The RD theory along with the Gierer-Meinhardt's activator-inhibitor model has been employed in the present study to understand the underlying principles in the formation of the alternating violet and white bands in Passion flower. Realistic values for the kinetic and diffusion parameters were chosen for the purpose. The diffusion coefficient for the inhibitor was taken to be significantly larger than that for the activator. In other words, the inhibitor was allowed to move faster than the activator, controlling the quadratic growth of the activator and resulting in an oscillation of the concentrations of both species. Interestingly, the alternation of the observed bands of violet and white colors is NOT uniform along the length of the filaments in PI. The width of the white band decreases initially on going away from the centre, then increases and finally decreases. The width of the violet band, on the other hand, increases initially in going away from the centre and finally takes over almost completely. By varying the relative initial concentrations of the activator and the inhibitor and varying their diffusion coefficients, it is shown that the alternating bands of violet and white in PI can be understood in terms of the activator-inhibitor model, with the inhibitor moving faster than the activator.

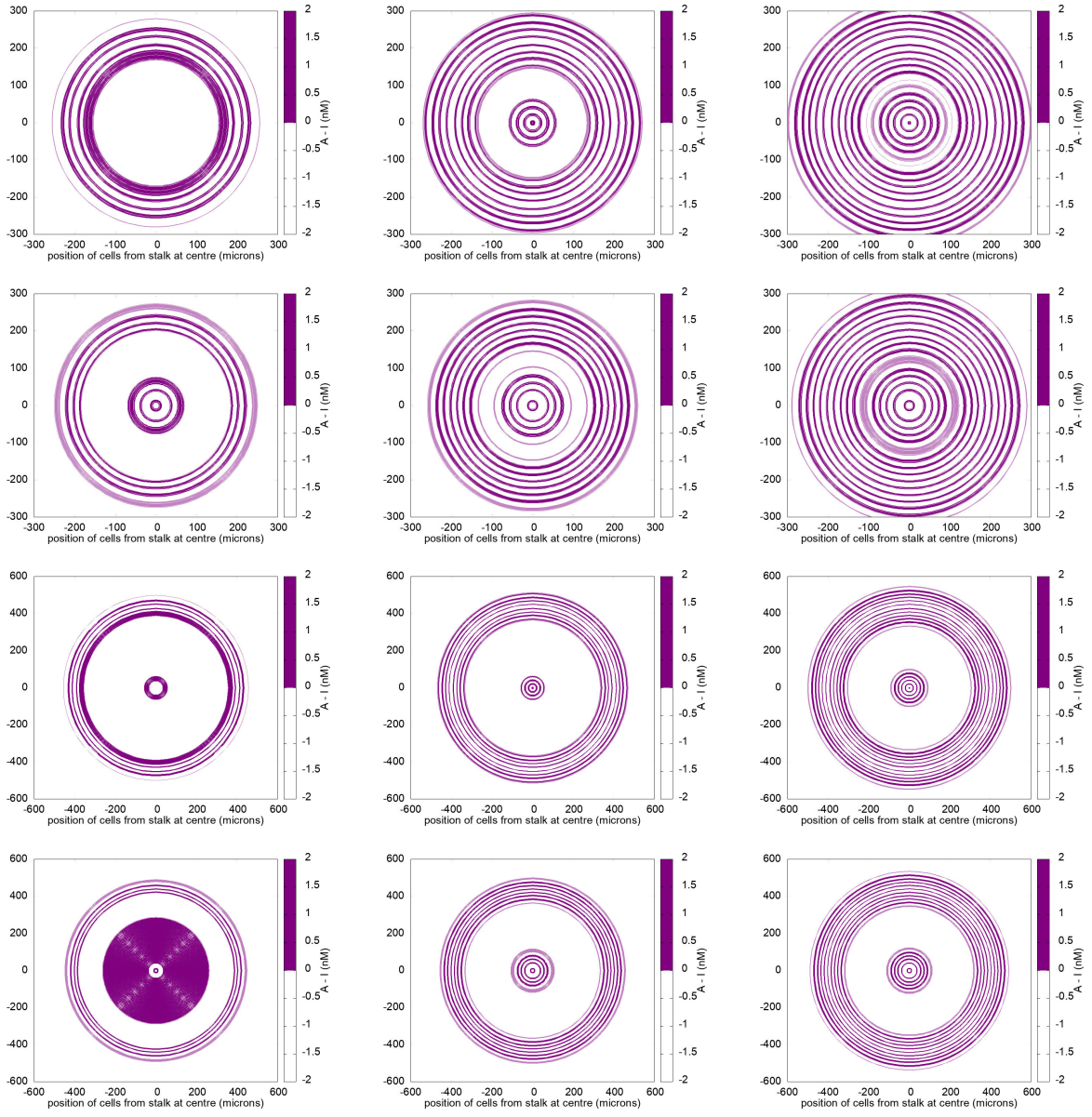

Figure 8: Spatio-temporal evolution of A and I in (x, y) coordinates at intervals of 1000 s for the initial conditions IC3-IC6. The top three panels are for IC3, and the subsequent sets of three panels are for IC4, IC5 and IC6, respectively.

While the violet color of PI is attributed to anthocyanins based on chemical analysis, the biochemical pathway for its formation is yet to be determined. It is hoped that our study would provide an impetus to the study of the flower formation in PI and the colored patterns therein.

Acknowledgement

The authors are grateful to Dr. Amitabh Nandi and Dr. Vinod Gaur for their suggestions in the initial stages of the work and Dr. T. Ramasami for helpful discussions while preparing the

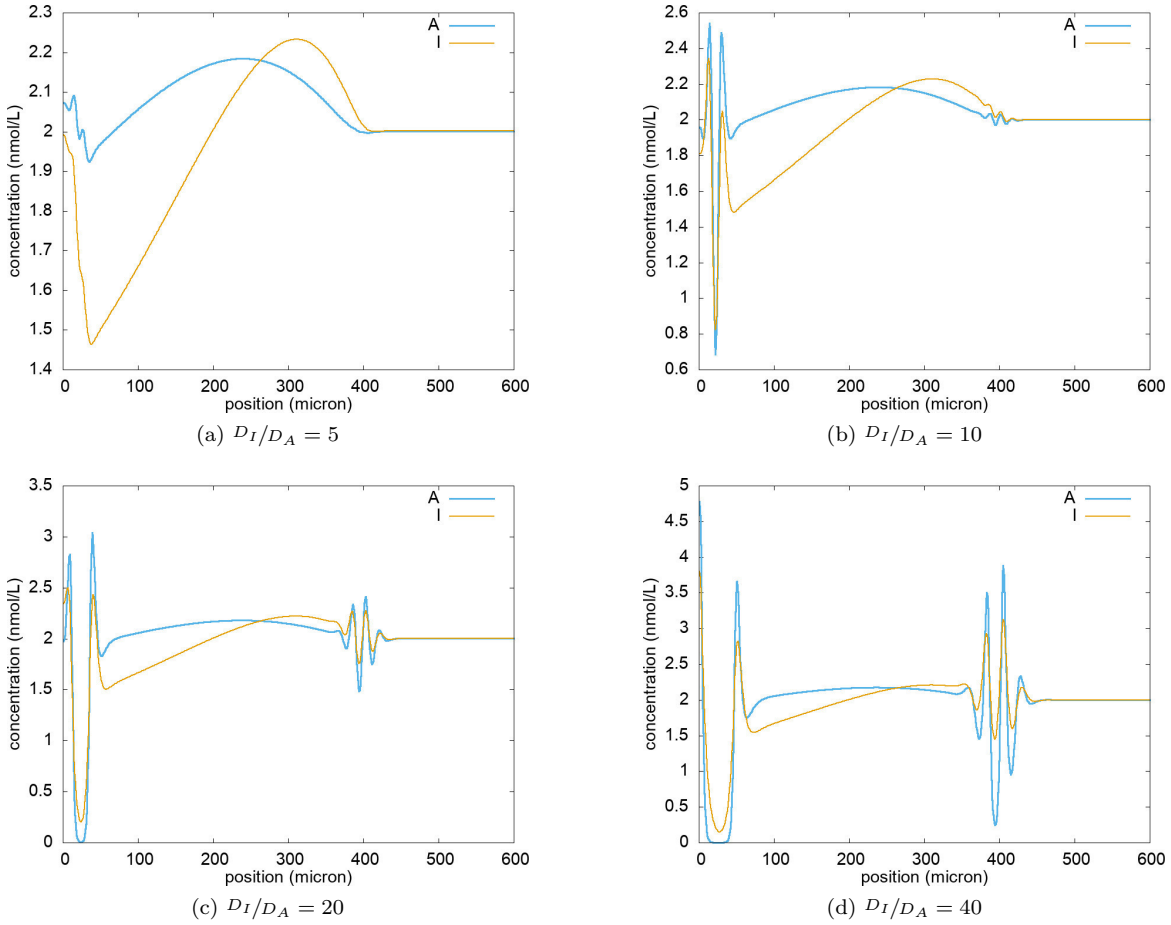

(a) $^{D_I}/_{D_A} = 5$ (b) $^{D_I}/_{D_A} = 10$

(c) $^{D_I}/_{D_A} = 20$ (d) $^{D_I}/_{D_A} = 40$

Figure 9: Snapshots of the system at 1000 s obtained using different values of the relative diffusion coefficients ($^{D_I}/_{D_A}$) for the initial condition IC6, with the concentration of A and I (in nM units) plotted along the y-axis.

manuscript. NS is grateful to the Department of Science and Technology, New Delhi for a J C Bose National Fellowship (2006-2016).

Bibliography

Ball, P. (2016). *Patterns in nature: why the natural world looks like the way it does*. University of Chicago Press, Chicago.

Bhati, A. P. (2014). Understanding the mechanism of pattern formation in passion flower. Master's thesis, Indian Institute of Science Education and Research Mohali.

Bhatnagar, S. S. and Sehgal, J. L. (1926). *Kolloid Zeit*, 39:264.

Chailakhyan, M. K. (1936). New facts in support of the hormonal theory of plant development. In *Dokl. Akad. Nauk SSSR*, volume 4, pages 77–81.

Culbertson, C. T., Jacobson, S. C., and Ramsey, J. M. (2002). *Talanta*, 56:365–373.

Field, R. J. and Noyes, R. M. (1977). Oscillations in chemical systems. 18. mechanisms of chemical oscillators: Conceptual bases. *Accounts of Chemical Research*, 10(6):214–221.

Gierer, A. and Meinhardt, H. (1972). *Kybernetik*, 12:30–39.

Goyal, S., Reji, R., Tripathi, S. S., and Sathyamurthy, N. (2019). Synchronous pulsed flowering in passion flower (*Passiflora incarnata*). *Current Science*, 117(7):1211–1216.

Hearn, D. J. (2019). Turing-like mechanism in a stochastic reaction-diffusion model recreates three dimensional vascular patterning of plant stems. *PloS one*, 14(7):e0219055.

Kondo, S. and Asai, R. (1995). A reaction–diffusion wave on the skin of the marine angelfish *Pomacanthus*. *Nature*, 376(6543):765–768.

Kondo, S. and Miura, T. (2010). Reaction-diffusion model as a framework for understanding biological pattern formation. *Science*, 329(5999):1616–1620.

Krug, H.-J. and Brandtstädter, H. (1999). Morphological characteristics of liesegang rings and their simulations. *The Journal of Physical Chemistry A*, 103(39):7811–7820.

Lang, A. and Melchers, G. (1943). Die photoperiodische reaktion von *Hyoscyamus niger*. *Planta*, 33(5. H):653–702.

Lotka, A. J. (1910). Contributions to the theory of periodic reactions. *The Journal of Physical Chemistry*, 14(3):271–274.

McGuigan, H. and Brough, G. A. (1923). Rhythmic banding of precipitates (liesegang's rings). *Journal of Biological Chemistry*, 58(2):415–423.

Meinhardt, H. (1982). *Models of biological pattern formation*. Academic Press, New York.

Meinhardt, H. (1995). Dynamics of stripe formation. *Nature*, 376(6543):722–723.

Meinhardt, H. (2009). *The algorithmic beauty of sea shells, 4th ed.* Springer-Verlag, Berlin.

Murray, J. D. (2003). *Mathematical Biology, 3rd ed.*, volume II. Springer, Berlin, Heidelberg.

Painter, K., Maini, P., and Othmer, H. G. (1999). Stripe formation in juvenile pomacanthus explained by a generalized turing mechanism with chemotaxis. *Proceedings of the National Academy of Sciences*, 96(10):5549–5554.

Ramasastry, S. S., Silori, Y., Chawla, S., De, A. K., and Sathyamurthy, N. (2021). preprint.

Rashevsky, N. (1961). *Mathematical principles in biology and their applications*. Thomas.

Singh, A. P. and Nüsslein-Volhard, C. (2015). Zebrafish stripes as a model for vertebrate colour pattern formation. *Current Biology*, 25(2):R81–R92.

Stern, K. H. (1954). The liesegang phenomenon. *Chemical Reviews*, 54(1):79–99.

Thomas, D. and Kernezev, J. P., editors (1975). *Analysis and Control of Immobilized Enzyme Systems*. Springer-Verlag, Berlin-Heidelberg-New York.

Turing, A. M. (1952). *Phil. Trans. of Roy. Soc. (London) B*, 237:37–72.

van Roekel, H. W. H., Rosier, B. J. H. M., Meijer, L. H. H., Hilbers, P. A. J., Markvoort, A. J., Huck, W. T. S., and de Greef, T. F. A. (2015). Programmable chemical reaction networks: emulating regulatory functions in living cells using a bottom-up approach. *Chemical Society Reviews*, 44(21):7465–7483.

Williams, R. B. and Murdoch, M. B. (1966). Phytoplankton production and chlorophyll concentration in the beaufort channel, north carolina. Technical report, Bureau of Commercial Fisheries, Radiobiological Laboratory, Beaufort, North Carolina.

Winfree, A. T. (1972). Spiral waves of chemical activity. *Science*, 175(4022):634–636.

Winter, R. B., Berg, O. G., and Hippe, P. H. v. (1981). Diffusion-driven mechanisms of protein translocation on nucleic acids. 3. the escherichia coli lac repressor-operator interaction: Kinetic measurements and conclusions. *Biochemistry*, 20:6961–6977.

Yuan, Y.-W., Rebocho, A. B., Sagawa, J. M., Stanley, L. E., and Bradshaw, H. D. (2016). Competition between anthocyanin and flavonol biosynthesis produces spatial pattern variation of floral pigments between mimulus species. *Proceedings of the National Academy of Sciences*, 113(9):2448–2453.

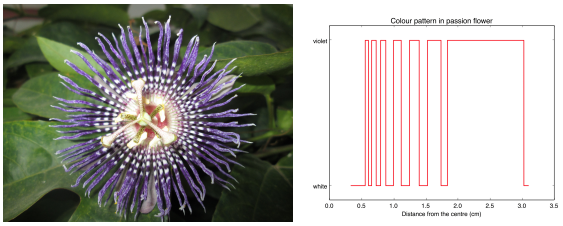

Figure for TOC entry